2-2010

Ultrabroad-bandwidth arbitrary radiofrequency waveform generation with a silicon photonic chip-based spectral shaper

Maroof H. Khan
Birck Nanotechnology Center, Purdue University, mhkhan@purdue.edu

Hao Shen
Purdue University - Main Campus, shen17@purdue.edu

Yi Xuan
Purdue University - Main Campus, yxuan@purdue.edu

Lin Zhao
Purdue University - Main Campus, linzhao@purdue.edu

Shijun Xiao
Purdue University - Main Campus

See next page for additional authors

Khan, Maroof H.; Shen, Hao; Xuan, Yi; Zhao, Lin; Xiao, Shijun; Leaird, Daniel E.; Weiner, Andrew M.; and Qi, Minghao, "Ultrabroad-bandwidth arbitrary radiofrequency waveform generation with a silicon photonic chip-based spectral shaper" (2010). *Birck and NCN Publications.* Paper 682.
http://dx.doi.org/10.1038/NPHOTON.2009.266

nature photonics

ARTICLES

PUBLISHED ONLINE: 17 JANUARY 2010 | DOI: 10.1038/NPHOTON.2009.266

Ultrabroad-bandwidth arbitrary radiofrequency waveform generation with a silicon photonic chip-based spectral shaper

Maroof H. Khan[1,2‡], Hao Shen[1,3‡], Yi Xuan[1,3], Lin Zhao[1,3], Shijun Xiao[1,3†], Daniel E. Leaird[1,3], Andrew M. Weiner[1,3*] and Minghao Qi[1,3*]

Ultrabroad-bandwidth radiofrequency pulses offer significant applications potential, such as increased data transmission rate and multipath tolerance in wireless communications. Such ultrabroad-bandwidth pulses are inherently difficult to generate with chip-based electronics due to limits in digital-to-analog converter technology and high timing jitter. Photonic means of radiofrequency waveform generation, for example, by spectral shaping and frequency–time mapping, can overcome the bandwidth limit in electronic generation. However, previous bulk optic systems for radiofrequency arbitrary waveform generation do not offer the integration advantage of electronics. Here, we report a chip-scale, fully programmable spectral shaper consisting of cascaded multiple-channel microring resonators, on a silicon photonics platform that is compatible with electronic integrated circuit technology. Using such a spectral shaper, we demonstrate the generation of burst radiofrequency waveforms with programmable time-dependent amplitude, frequency and phase profiles, for frequencies up to 60 GHz. Our demonstration suggests potential for chip-scale photonic generation of ultrabroad-bandwidth arbitrary radiofrequency waveforms.

Radiofrequency (RF) technology is ubiquitous in systems such as radar, remote sensing and wireless communications. Conventionally, RF systems operate at low instantaneous bandwidth with continuous-wave signals possessing a well-defined (although perhaps slowly tunable) centre frequency. Recently, however, there has been increased interest in pulse-like RF systems that can operate simultaneously over an ultrawide band, for example, 3.1 to 10.6 GHz for high-data-rate indoor communications[1]. The ability to generate arbitrary ultrabroad-bandwidth RF waveforms may lead to new opportunities and significant performance enhancement in applications ranging from extremely high-bandwidth secure wireless communications[2,3] to impulse radar[4,5]. Unfortunately, high-frequency (for example, ~10–60 GHz), ultrabroad-bandwidth arbitrary waveforms cannot be readily generated by electronic means due to limits in digital-to-analog converter technology and high timing jitter. Recently, arbitrary burst RF waveforms have been programmably generated using ultrafast photonics, for example, by spectral shaping[6–9] and frequency–time mapping[8,9] of femtosecond laser pulses. A critical bottleneck in such setups, however, is the use of a bulk optics pulse shaper[6] as the spectral shaping element, which requires accurate alignment and high environmental stability, thus hampering widespread implementation. Here, we demonstrate an ultracompact, fully programmable, integrated spectral shaper consisting of cascaded multiple-channel microring resonators[10–14]. It has a footprint of 100 μm × 1,200 μm (excluding electrical contact pads) on a silicon-on-insulator (SOI) platform[15] that is compatible with electronic integrated circuit technology. We achieved complete RF waveform control, including amplitude, frequency and phase, for frequencies up to 60 GHz, by thermally tuning both the resonant frequencies and the coupling strengths of the microring resonators. We anticipate our demonstration to be a starting point for the miniaturization of ultrabroad-bandwidth microwave (or RF) photonics and for system-level applications of silicon photonics.

At the outset we note that optical pulse shapers have previously been integrated by adapting silica planar lightwave circuit (PLC) technology[16,17]. Such silica PLCs are much larger in size than silicon photonics and lack potential for direct electronic integration, and pulse-shaping demonstrations, although interesting for ultrafast optical waveform generation, do not address the spectral shaping functionality crucial for RF arbitrary waveform generation (AWG) via frequency–time mapping. Meanwhile, ultrawide-bandwidth RF pulse generation has been demonstrated by frequency–time mapping of femtosecond pulses spectrally shaped using compact fibre Bragg grating devices[18]; however, these devices lack the programmability needed for AWG applications.

Device and waveform generation concept

Figure 1 illustrates our first-generation system setup and representative results. A short pulse (100 fs in duration) from a mode-locked fibre laser is amplified and coupled into a silicon waveguide via lensed single-mode fibre tips. In the frequency domain, the short pulse has a large bandwidth, and in our case covers a wavelength band from 1,525 to 1,610 nm (Fig. 1a). Our on-chip spectral shaper consists of eight cascaded microring resonators (Fig. 1b), all in an add–drop configuration[12]. Each microring will selectively transfer the optical power at its resonance wavelength from the through-port waveguide to the drop-port waveguide, thus creating a dip in the through-port spectrum (Fig. 1c). The rings in Fig. 1b are shown with different colours, indicating that each ring is

[1]Birck Nanotechnology Centre, Purdue University, 1205 West State Street, West Lafayette, Indiana 47907, USA, [2]Department of Physics, Purdue University, 525 Northwestern Avenue, West Lafayette, Indiana 47907, USA, [3]School of Electrical and Computer Engineering, Purdue University, 465 Northwestern Avenue, West Lafayette, Indiana 47907, USA; †Present address: Department of Electrical Engineering and Computer Science, Northwestern University, 2145 Sheridan Road, Evanston, Illinois 60208, USA.; ‡These authors contributed equally to this work. *e-mail: mqi@purdue.edu; amw@purdue.edu

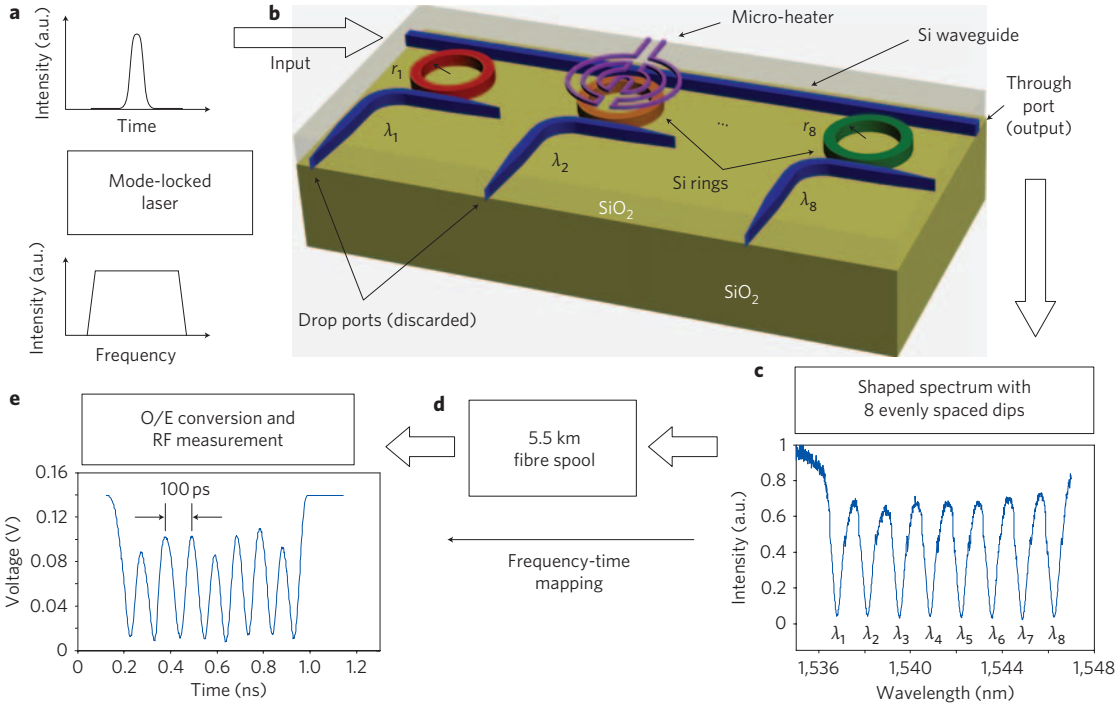

Figure 1 | Schematic and representative results of the chip-based photonic RF waveform generation. a, The input light source is a mode-locked and amplified femtosecond laser, which has a broadband spectrum extending from 1,525 to 1,610 nm. **b**, The integrated spectral shaper consists of eight cascaded microring resonators, each having a slightly different resonant wavelength (indicated by their different colours). The resonance wavelengths, λ_1, λ_2, ... , λ_8 can be individually tuned by the micro-heaters above the rings. **c**, The through-port optical spectrum shows eight equally spaced dips, when the ring resonance wavelengths, λ_1, λ_2, ... , λ_8, are tuned to be equally spaced. **d**, Frequency–time mapping is achieved with a 5.5-km fibre spool. **e**, Optical/electronic (O/E) conversion of the optical signal with a high-speed photodetector shows an RF pulse waveform burst with a 10 GHz fundamental carrier frequency.

designed to have a slightly different perimeter and therefore a different resonant wavelength. A micro-heater is placed above each ring (see Methods section for fabrication procedure) and can locally and independently control the temperature of each individual ring resonator. Owing to the large thermo-optical effect in silicon[19], the resonance wavelength of each resonator can be tuned. Figure 1c shows the optical transmission spectrum for an experiment in which we tuned the rings to achieve equal spacing in resonance wavelengths.

After the on-chip spectral shaper, the output optical signal passes through a 5.5 km single-mode fibre spool (Fig. 1d). The linear chromatic dispersion in the fibre causes different frequency components to propagate at different speeds. The ultrashort pulse envelope is therefore broadened, resulting in a time-domain profile that is a scaled version of the frequency spectrum (a process called frequency–time mapping[8,9]). The optical intensity envelope is then converted to an RF electrical signal with a high-speed photodiode. The time-domain electrical signal (Fig. 1e), measured using a sampling oscilloscope, has the same shape as the optical power spectrum (Fig. 1c), confirming frequency–time mapping operation. In this example the RF signal was programmed to be a single frequency waveform burst with a fundamental frequency of 10 GHz. Although quite simple, this experiment constitutes an important first demonstration of controllable RF waveform generation using microring silicon photonics. Generation of more complex waveforms beyond the capabilities of electronic solutions will be presented later. Note that manipulation of the optical spectrum followed by frequency–time mapping and photodetection may be considered as belonging to the general class of microwave photonic discrete time filters[20–22]; in this setup, each microring functions as an independent filter tap.

Unfortunately, heating the ring itself has little effect on the coupling efficiency from the straight waveguide into the ring, which means the depth of dips at λ_1, λ_2, ... , λ_8, or the amplitudes of spectral attenuation cannot be controlled. This significantly limits the variety of waveforms that can be generated. In a second-generation design, Mach–Zehnder (MZ) input couplers were formed at the through port of every microring (Fig. 2a,b). By thermally tuning the phase shift between the two arms, the coupling coefficient into a ring, and therefore its loaded quality factor, can be changed[23]. For each resonant frequency, full tuning from the ON state (no dip) to the OFF state (a deep dip) can be achieved by controlling the phase shift applied to the MZ arm from 0 to π. Figure 2c shows that one can tune the attenuation of one resonance (channel 2) from 0 to 27 dB without appreciably affecting the adjacent resonance (channel 1). Furthermore, to increase experimental flexibility, in this device design, waveguides representing both a common through port and a common drop port were brought to the output of the chip. As a result, the spectrally shaped optical pulse can now be collected either at the through port or at the common drop port.

Results

Figure 3a–f demonstrates the coordinated control of individual peak amplitudes within an RF waveform. For these data we took the optical signals from the common drop port (Fig. 2a), for which the optical spectrum consists of peaks from a background of zero (Fig. 3a–c) rather than dips from a high background (Fig. 1e). We were able to program our spectral shaper chip for 10 GHz waveforms with either progressively decreasing (Fig. 3a) or increasing (Fig. 3b) peak amplitudes. Such amplitude modulation capability has a number of applications. One example is apodization, an important technique used in signal and filter design with which side lobes in the Fourier transform domain are suppressed[24,25]. We first controlled both the amplitude and spacing of individual peaks to achieve an RF signal centred at 10 GHz under an approximately flat-topped envelope (Fig. 3c). Owing to the abrupt amplitude changes at the leading and trailing edges of the burst, the

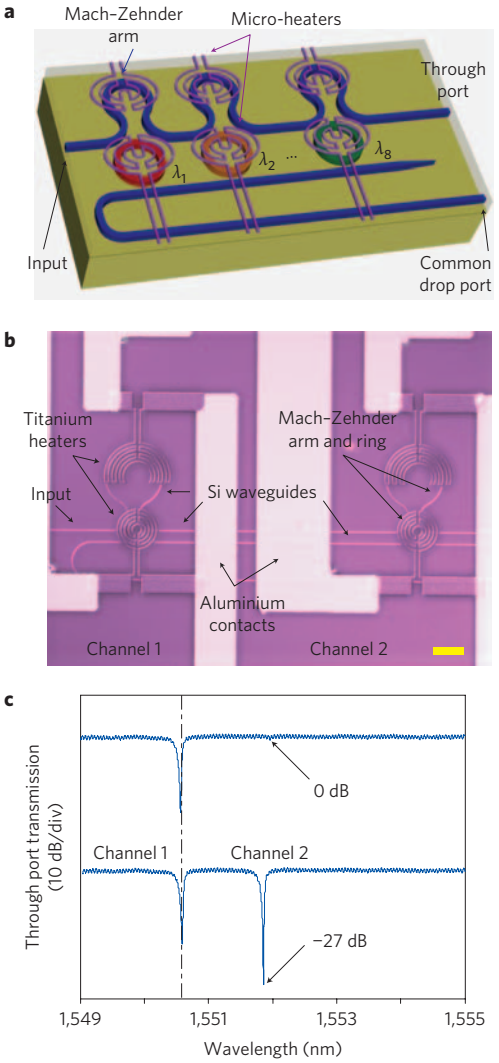

Figure 2 | Controlling the attenuation of individual frequency components in the integrated spectral shaper. a, Mach–Zehnder arms are incorporated in the through-port waveguide near the rings. Unlike in Fig. 1b, the signals can now be collected from either the through port or the common drop port. **b**, An optical image showing two sets (or channels) of finished ring resonators with micro-heaters and contact pads. Scale bar, 20 μm. **c**, Demonstration of the independent control of through-port attenuation.

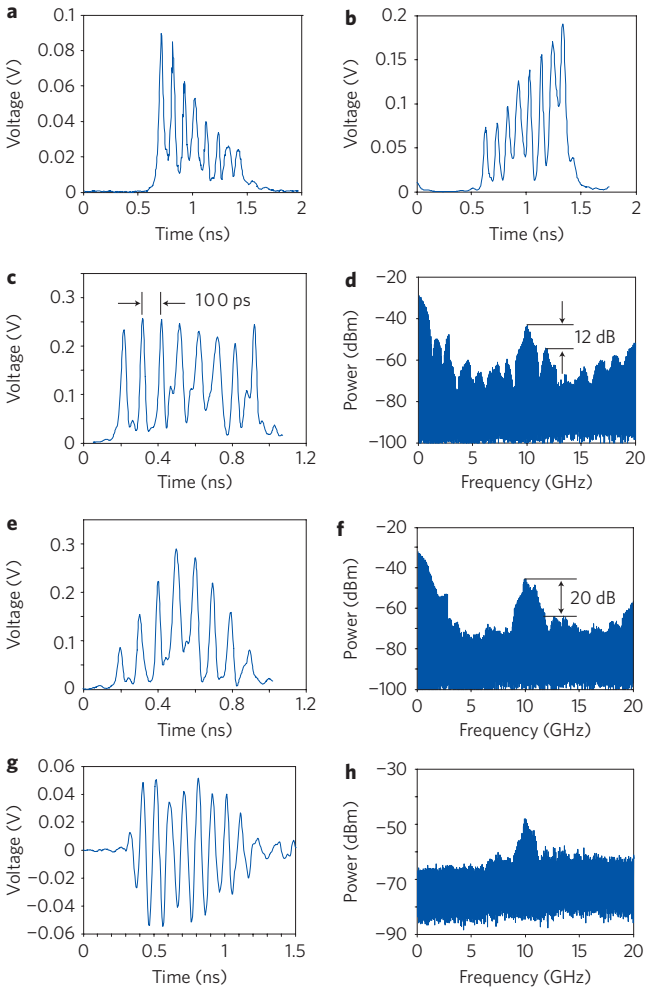

Figure 3 | Controlling the amplitudes of individual peaks in 10 GHz RF waveforms. a,**b**, Coordinated amplitude control of the RF waveforms. **c**–**f**, The 10 GHz waveforms and RF power spectra before (**c**,**d**) and after (**e**,**f**) apodization. **g**,**h**, Bi-polar waveform and power spectrum of a 10 GHz RF burst after a high-pass RF filter.

corresponding RF power spectrum has a side-lobe suppression of only −12 dB (Fig. 3d). On the other hand, an apodized waveform, programmed such that the peaks are gradually attenuated at the leading and trailing edges of the RF burst (Fig. 3e), demonstrates a significantly improved side-lobe suppression of −20 dB (Fig. 3f). Such improvement in side-lobe suppression is consistent with simulations. The large optical power at low (baseband) RF frequencies is a result of the positive-definite nature of the photodetector output signal, and can be eliminated by applying a high-pass RF filter. Figure 3g,h shows the bipolar RF signal obtained after filtering. The −3 dB frequency bandwidth of the RF burst is 400 MHz, which is limited by the number of RF oscillations (eight in our case).

With the capability of completely controlling wavelength and amplitude tuning, we start to generate various waveforms, particularly those that are very difficult, if not impossible, to generate by electronic means at such a high frequency. Figure 4a shows a 10 GHz waveform with a π-phase shift between the four cycles on the right and the four on the left. A doublet in the RF power spectrum with a dip at 10 GHz (Fig. 4b) is formed by the interference between the left four cycles and the right four cycles, and is a strong indication of the phase shift within the pulse burst. Figure 4c shows a waveform with multiple π-phase shifts. The ability to generate user-defined, phase-coded RF waveforms over an ultrawide bandwidth may contribute to the extension of spread spectrum communications techniques such as code-division multiple-access (CDMA), popular at lower centre frequencies and bandwidths for cellular radio, to ultrawide-bandwidth wireless systems at much higher data rates[26].

Our scheme can be easily scaled up to higher frequencies. Here, we first demonstrate a 'two-tone' waveform with an abrupt frequency change from 60 to 40 GHz (Fig. 4d). Such an abrupt frequency shift is beyond the capability of current generation of electronic circuitry, but can be conveniently achieved with our method by reducing the fibre stretcher length and re-tuning the spacing between the resonance wavelengths of the adjacent rings. Figure 4e,f shows a 60 GHz waveform with a π-phase shift and the corresponding power spectrum with a strong dip near 60 GHz. Interestingly, these 60 GHz waveform examples are already pushing the edge of time-domain electronic measurement instrumentation (our sampling oscilloscope is specified only to 50 GHz). These demonstrations could contribute to the realization of multi-gigahertz bandwidth in wireless local area networks, portable multimedia streaming and vehicular networks, as there is around 7 GHz of internationally available, unlicensed

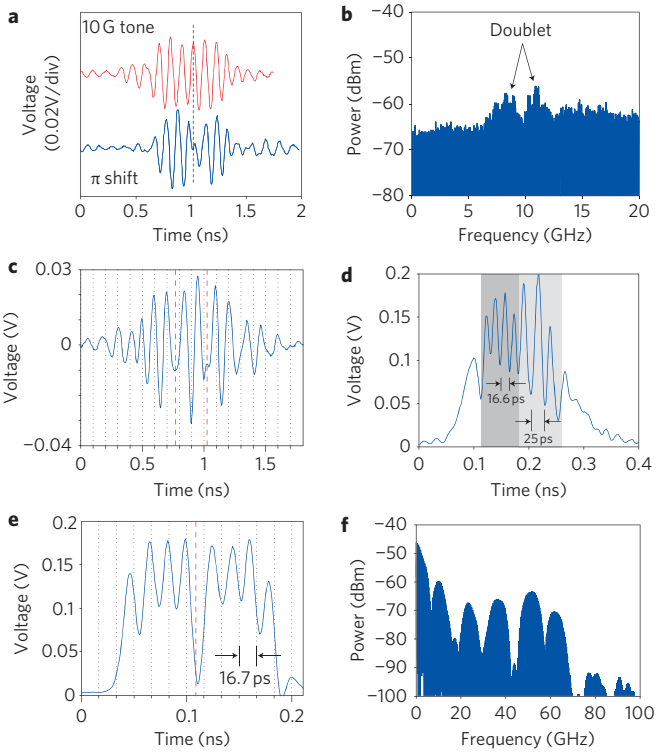

Figure 4 | Phase and frequency control in waveforms up to 60 GHz fundamental frequencies. a,**b**, RF waveform and spectrum of a 10-GHz pulse burst with a π-phase shift. **c**, A 10 GHz RF burst with multiple π-phase shifts. The vertical lines are visual guides to help determine the phases of the peaks. The two intentionally programmed phase shifts are marked with red dashed lines. **d**, A two-tone RF waveform with an abrupt frequency change from 60 to 40 GHz (without a high-pass RF filter). This was achieved by shrinking the length of the fibre stretcher and reprogramming the resonance wavelengths of the rings. **e**,**f**, RF waveform and spectrum (calculated from the time-domain data) of a 60 GHz pulse burst with a π-phase shift.

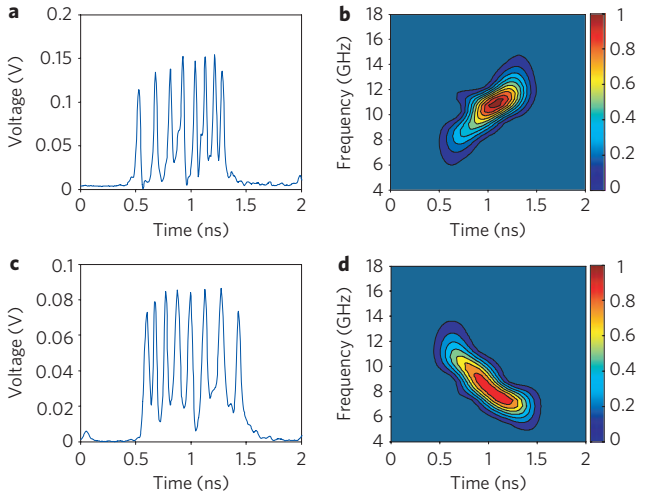

Figure 5 | Generation of chirped RF waveforms. a,**b**, RF waveform and spectrogram of an up-chirped signal. **c**,**d**, RF waveform and spectrogram of a down-chirped signal. The spectrograms, which describe the time distribution of the RF frequency content, clearly show monotonic frequency modulation. The colours indicate the relative spectral intensity of the frequency component, with red being strongest and blue weakest. Low-frequency content below 4 GHz is not shown in these spectrograms.

spectrum surrounding the 60 GHz carrier frequency[3]. It is also interesting to note that higher frequency requires a shorter length in the dispersive medium, thus reducing the total weight of the waveform generation equipment. In principle, the low loss and large dispersion in compact silicon waveguides[27,28] may allow integration of frequency–time mapping onto the chip for terahertz waveform generation applications.

Figure 5 shows examples of ultrabroad-bandwidth frequency-modulated waveforms, for which the sign of the frequency modulation (or 'chirp') can be programmed to sweep from low to high frequency (up-chirp, Fig. 5a) or from high to low (down-chirp, Fig. 5c). Frequency modulated signals are commonly used, for example, in chirped radar[29], in which the bandwidth of the radar signal is spread in time to reduce the peak power to energy ratio of the transmitted pulse. Figure 5b and d show spectrograms of the up-chirp and down-chirp waveforms, respectively. Spectrograms are an example of a joint time–frequency distribution, an analysis tool used to characterize signals for which the frequency content is varying in time[30]. (Musical scores, which specify a series of musical notes as a function of time, may also be regarded as a type of spectrogram.) Here, the different slopes of the spectrograms clearly indicate the ability to achieve either up- or down-chirp. The range of the frequency sweep, of the order of 8 GHz, is more than an order of magnitude higher than conventional chirped radars operating at similar centre frequencies. Accordingly, waveforms such as those shown here offer intriguing potential for enhanced range resolution, which is inversely proportional to bandwidth. As noted above, further increases in frequency sweep and RF bandwidth may be achieved simply by using shorter dispersive stretchers.

Discussion

Compared to electronic means of RF waveform generation, our photonically assisted RF–AWG makes possible RF waveforms with much higher instantaneous bandwidth, cycle-by-cycle frequency control, and flexible frequency band (for example, 10–60 GHz, limited only by the speed of photodetectors). Furthermore, by using special optical-to-electrical converters, such as ultrafast photoconductive switches, it should be possible to scale our RF–AWG approach into the terahertz region, as previously demonstrated using bulk optics pulse shapers[31].

Note that our waveforms currently have a limited number of cycles. However, with the availability of silicon microring resonators with ultranarrow resonant linewidth[27,28] and ultracompact footprint, a large number of microrings could be integrated onto a single silicon chip to provide a large number of cycles for each RF burst. The updating speed of our chip-based RF waveform generator is currently limited by the speed of thermal tuning, which is typically in the millisecond to microsecond range[32], but can be improved to 1 μs or below if direct Joule heating of silicon is adopted[33–35]. Moreover, with recent demonstration of fast electronic modulation in ring resonators[36,37], one can envision RF generation with multi-gigahertz update speeds, resulting in a RF waveform agility far beyond the means of current electronic solutions. The total optical loss of the spectral shaper chip is typically 25 dB, with a main contribution from the fibre-to-chip coupling (~10 dB for each coupler). Efficient coupling schemes such as tapers[27,38,39] and grating couplers[40,41], which have demonstrated fibre-to-chip coupling with losses down to 0.5 dB per coupler[38], will be incorporated in future chips to improve the power level of the output signal and to increase the signal-to-noise ratio.

We believe that the arbitrary RF waveform generation application first introduced here is particularly suitable for the development of systems-on-a-chip based on SOI ring resonator arrays, because the requirements for linewidth, accurate frequency control and out-of-band suppression are less stringent than for other commonly cited applications such as dense wavelength-division demultiplexing. Note

also that a photonics approach involving a bulk optics shaper has recently been demonstrated for programmable RF phase filtering and pulse compression over an unprecedented (~15 GHz) RF bandwidth[42]. Thus, microring resonator devices similar to those described here offer prospects not only for waveform generation, but also for integrated realization of the spectral shaping function crucial for novel photonics-enabled ultrabroad-bandwidth RF signal processing.

Methods

Fabrication. We fabricated the microrings on an SOI wafer (from SOITEC) with a 250-nm-thick top silicon layer and 3 μm of buried oxide. Microring resonators were patterned with high-resolution electron-beam lithography (Vistec VB6) with a beam step size of 2 nm. The radius of a typical microring resonator is ~5 μm and the free spectral range of this resonator in the C-band is ~16 nm. The resonators were formed after reactive-ion etching in a chlorine/argon plasma. An over-cladding of 1.2 μm silicon dioxide was deposited in a plasma-enhanced chemical vapour deposition tool and subsequently annealed in a rapid thermal processing tool. Titanium micro-heaters with a resistance of 1.2 kΩ were evaporated on top of the silicon dioxide over each microring resonator and MZ arm. The large contact pads shown in Fig. 2b were made by electron-beam evaporation of 1 μm aluminium.

Generation and measurement of RF waveforms. A home-made erbium fibre femtosecond mode-locked laser (~100 fs) with 50 MHz repetition rate was used as the source, with a spectral content from 1,525 to 1,610 nm. The source was guided into and out of the silicon waveguide by single-mode tapered lensed fibres. The fibres were fixed on *xyz*-nanopositioning stages. A fibre-based polarization controller was used before the input lensed fibre to maintain the quasi transverse electric (TE) mode. Spectrally shaped pulses were collected either at the through port (for waveforms shown in Figs 1c,e, 2c and 4a–4d) or the common drop port (the remaining waveforms). The output signal was then coupled into a length (~5.5 km for RF waveforms of 10 GHz fundamental frequency) of single-mode fibre (SMF) to provide dispersion for frequency–time mapping. Two erbium-doped fibre amplifiers (EDFAs) were used to compensate the fibre-to-fibre loss (typically 25 dB). A free space bandpass filter with a −3 dB bandwidth of 12 nm was used to select one free spectral range of the microring spectra (except for the results shown in Fig. 1c,e). The shaped optical pulses were then guided into a photodiode with 22 GHz or 60 GHz bandwidth to generate the electrical waveform. In some experiments (see Figs 3 g,h and 4a–c), a high-pass RF filter with a stop band below 5 GHz was applied after the photodiode to suppress low-frequency components. The RF waveforms were acquired with a communication signal analyser (Tek803C or HP54124A) and RF spectrum analyser (Agilent 8565EC).

The heaters on the chip were controlled individually with 16 current sources (max 35 V, 3 A output). A compact multihead probe (Cascade DCQ-16) with 250-μm spacing between the probe heads was used. The chip was glued to an aluminium block with thermal grease to dissipate the extra heat on the chip, and to suppress the thermal cross-talk, which is ~3% for adjacent microrings. The spectral response of the microring resonators was characterized with a tunable laser (Agilent 81940A) and an optical power sensor (Agilent 81634B), with a scanning resolution of 0.01 nm. In waveform generation experiments using short-pulse inputs, optical spectra were first acquired with an optical spectral analyser (Ando AQ6317B), which allows one to interactively adjust the individual heaters to achieve the desired accuracy of wavelength spacing, especially when thermal cross-talk is present.

Calculation of the spectrograms and RF power spectrum. The spectrograms of chirped signals (Fig. 5) were calculated numerically using the following:

$$S_e(\omega,\tau)=\left|\int e(t)g(t-\tau)e^{-j\omega t}\,\mathrm{d}t\right|^2$$

where $e(t)$ is the RF burst and $g(t)$ a gating function. Here, the gating function is chosen to be Gaussian, that is, $g(t)=\exp(-t^2/t_p^2)$ with $t_p=0.25$ ns, and the delay τ was adjusted from 0 to 2 ns. The squared magnitude of the fast Fourier transform (FFT) of the windowed RF signal was then computed to obtain the spectrogram.

The RF power spectrum for the 60 GHz waveform (Fig. 4f) was derived by taking the FFT of the windowed time-domain signal shown in Fig. 4e and then plotting the magnitude squared. The calculation does not include noise associated with the EDFAs and photodiodes outside the time window of the RF waveform; thus, the calculated power spectrum has lower noise level than those measured directly on an RF spectral analyser.

Received 27 May 2009; accepted 25 November 2009; published online 17 January 2010

References

1. Reed, J. H. *An Introduction to Ultra Wideband Communication Systems* (Prentice-Hall, 2005).
2. Win, M. Z. & Scholtz, R. A. Ultra-wide bandwidth time-hopping spread-spectrum impulse radio for wireless multiple-access communications. *IEEE Trans. Commun.* **48,** 679–691 (2000).
3. Daniels, R. C. & Heath, R. W. 60 GHz wireless communications: emerging requirements and design recommendations. *Veh. Technol. Mag.* **2,** 41–50 (2007).
4. Azevedo, S. & McEwan, T. E. Micropower impulse radar. *Science and Technology Review, Lawrence Livermore National Laboratory* 17–29 (1996).
5. Lee, J. S., Nguyen, C. & Scullion, T. A novel, compact, low-cost, impulse ground-penetrating radar for nondestructive evaluation of pavements. *IEEE Trans. Instrum. Meas.* **53,** 1502–1509 (2004).
6. Weiner, A. M. Femtosecond pulse shaping using spatial light modulators. *Rev. Sci. Instrum.* **71,** 1929–1960 (2000).
7. McKinney, J. D., Leaird, D. E. & Weiner, A. M. Millimeter-wave arbitrary waveform generation with a direct space-to-time pulse shaper. *Opt. Lett.* **27,** 1345–1347 (2002).
8. Chou, J., Han, Y. & Jalali, B. Adaptive RF-photonic arbitrary waveform generator. *IEEE Photon. Technol. Lett.* **15,** 581–583 (2003).
9. Lin, I. S., McKinney, J. D. & Weiner, A. M. Photonic synthesis of broadband microwave arbitrary waveforms applicable to ultra-wideband communication. *IEEE Microw. Wirel. Compon. Lett.* **15,** 226–228 (2005).
10. Little, B. E., Chu, S. T., Haus, H. A., Foresi, J. & Laine, J. P. Micro-ring resonator channel dropping filters. *J. Lightwave Technol.* **15,** 998–1005 (1997).
11. Almeida, V. R., Barrios, C. A., Panepucci, R. R. & Lipson, M. All-optical control of light on a silicon chip. *Nature* **431,** 1081–1084 (2004).
12. Barwicz, T. *et al.* Microring-resonator-based add–drop filters in SiN: fabrication and analysis. *Opt. Express* **12,** 1437–1442 (2004).
13. Xiao, S., Khan, M. H., Shen, H. & Qi, M. Multiple-channel silicon micro-resonator based filters for WDM applications. *Opt. Express* **15,** 7489–7498 (2007).
14. Agarwal, A. *et al.* Fully programmable ring-resonator-based integrated photonic circuit for phase coherent applications. *J. Lightwave Technol.* **24,** 77–87 (2006).
15. Xiao, S., Khan, M. H., Shen, H. & Qi, M. Silicon-on-insulator micro-ring add–drop filters with free spectral ranges over 30 nm. *J. Lightwave Technol.* **26,** 228–236 (2008).
16. Miyamoto, D. *et al.* Waveform-controllable optical pulse generation using an optical pulse synthesizer. *IEEE Photon. Technol. Lett.* **18,** 721–723 (2006).
17. Takiguchi, K., Okamoto, K., Kominato, T., Takahashi, H. & Shibata, T. Flexible pulse waveform generation using silica-waveguide-based spectrum synthesis circuit. *Electron. Lett.* **40,** 537–538 (2004).
18. Wang, C. & Yao, J. Photonic generation of chirped millimeter-wave pulses based on nonlinear frequency-to-time mapping in a nonlinearly chirped fiber Bragg grating. *IEEE Trans. Microw. Theory Tech.* **56,** 542–553 (2008).
19. Li, H. H. Refractive index of silicon and germanium and its wavelength and temperature derivatives. *J. Phys. Chem. Reference Data* **9,** 561–658 (1980).
20. Capmany, J. & Novak, D. Microwave photonics combines two worlds. *Nature Photon.* **1,** 319–330 (2007).
21. Minasian, R. A. Photonic signal processing of microwave signals. *IEEE Trans. Microw. Theory Tech.* **54,** 832–846 (2006).
22. Yao, J., Zeng, F. & Wang, Q. Photonic generation of ultrawideband signals. *J. Lightwave Technol.* **25,** 3219–3235 (2007).
23. Popovic, M. A. *et al.* Transparent wavelength switching of resonant filters. In *Conference on Lasers and Electro-Optics/Quantum Electronics and Laser Science Conference and Photonic Applications Systems Technologies, OSA Technical Digest Series (CD)*, paper CPDA2 (Optical Society of America, 2007).
24. Harris, F. J. On the use of windows for harmonic analysis with the discrete Fourier transform. *Proc. IEEE* **66,** 51–83 (1978).
25. McKinney, J. D., Lin, I. S. & Weiner, A. M. Shaping the power spectrum of ultra-wideband radio-frequency signals. *IEEE Trans. Microw. Theory Tech.* **54,** 4247–4255 (2006).
26. Farhang, M. & Salehi, J. A. Spread-time/time-hopping UWB CDMA communication. In *IEEE International Symposium on Communications and Information Technology (ISCIT)*, Vol. 2, 1047–1050 (2004).
27. Vlasov, Y. A. & McNab, S. J. Losses in single-mode silicon-on-insulator strip waveguides and bends. *Opt. Express* **12,** 1622–1631 (2004).
28. Xiao, S., Khan, M. H., Shen, H. & Qi, M. Compact silicon microring resonators with ultra-low propagation loss in the C band. *Opt. Express* **15,** 14467–14475 (2007).
29. Klauder, J. R., Price, A. C., Darlington, S. & Albersheim, W. J. The theory and design of chirp radars. *Bell Syst. Tech. J.* **39,** 745–808 (1960).
30. Cohen, L. Time-frequency distributions—a review. *Proc. IEEE* **77,** 941–981 (1989).
31. Liu, Y., Park, S.-G. & Weiner, A. M. Terahertz waveform synthesis via optical pulse shaping. *IEEE J. Sel. Topics Quantum Electron.* **2,** 709–719 (1996).
32. Gan, F. *et al.* Maximizing the thermo-optic tuning range of silicon photonic structures. In *Photonics in Switching 2007*, 67–68 (2007).
33. Watts, M. R. *et al.* Adiabatic resonant microrings (ARMs) with directly integrated thermal microphotonics. In *Conference on Lasers and Electro-Optics/Quantum Electronics and Laser Science Conference and Photonic Applications Systems Technologies, OSA Technical Digest Series (CD)*, paper CPDB10 (Optical Society of America, 2009).

34. Vlasov, Y. A., O'Boyle, M., Hamann, H. F. & McNab, S. J. Active control of slow light on a chip with photonic crystal waveguides. *Nature* **438,** 65–69 (2005).
35. Geis, M. W., Spector, S. J., Williamson, R. C. & Lyszczarz, T. M. Submicrosecond submilliwatt silicon-on-insulator thermooptic switch. *IEEE Photon. Technol. Lett.* **16,** 2514–2516 (2004).
36. Xu, Q., Schmidt, B., Pradhan, S. & Lipson, M. Micrometre-scale silicon electro-optic modulator. *Nature* **435,** 325–327 (2005).
37. Xu, Q., Manipatruni, S., Schmidt, B., Shakya, J. & Lipson, M. 12.5 Gbit/s carrier-injection-based silicon micro-ring silicon modulators. *Opt. Express* **15,** 430–436 (2007).
38. Yamada, K. *et al*. Silicon wire waveguiding system: fundamental characteristics and applications. *Electron. Commun. Jpn, Part 2* **89,** 42–55 (2006).
39. Almeida, V. R., Panepucci, R. R. & Lipson, M. Nanotaper for compact mode conversion. *Opt. Lett.* **28,** 1302–1304 (2003).
40. Roelkens, G. *et al*. High efficiency diffractive grating couplers for interfacing a single mode optical fiber with a nanophotonic silicon-on-insulator waveguide circuit. *Appl. Phys. Lett.* **92,** 131101 (2008).
41. Shankar Kumar, S. *et al*. Highly efficient grating coupler between optical fiber and silicon photonic circuit. In *Conference on Lasers and Electro-Optics/ Quantum Electronics and Laser Science Conference and Photonic Applications Systems Technologies, OSA Technical Digest Series (CD)*, paper CTuC6 (Optical Society of America, 2009).
42. Hamidi, E. & Weiner, A. M. Phase-only matched filtering of ultrawideband arbitrary microwave waveforms via optical pulse shaping. *J. Lightwave Technol.* **26,** 2355–2363 (2008).

Acknowledgements

The authors would like to thank Li Fan for experimental assistance and for helpful discussions. The work was supported by the National Sciences Foundation under contract no. ECCS-0701448, the Defense Threat Reduction Agency under contract no. HDTRA1-07-C-0042 and by the Naval Postgraduate School under grant no. N00244-09-1-0068 under the National Security Science and Engineering Faculty Fellowship program. Any opinions, findings and conclusions or recommendations expressed in this publication are those of the authors and do not necessarily reflect the views of the sponsors.

Author contributions

M.H.K. led the fabrication of the spectral shaper chip with assistance from Y.X. and L.Z. H.S. set up the characterization apparatus and conducted the waveform generation and measurement with assistance from S.X. and D.E.L. M.Q. and A.M.W. conceived the idea and supervised the study. M.Q., A.M.W. and H.S. wrote the manuscript.

Additional information

The authors declare no competing financial interests. Reprints and permission information is available online at http://npg.nature.com/reprintsandpermissions/. Correspondence and requests for materials should be addressed to A.M.W. and M.Q.